Signal Processing 35 (1994) 33–40
Elsevier

High resolution imaging of continuously moving object using stepped frequency radar

Yingbo Hua
Department of Electrical and Electronic Engineering, University of Melbourne, Parkville, Victoria, 3052, Australia

Received 19 March 1992
Revised 30 July 1992 and 22 March 1993

Abstract. A stepped frequency inverse synthetic aperture radar is studied for imaging of continuously moving objects. The radar returns are shown to be a sum of two-dimensional complex exponentials over a small data aperture. A matrix pencil method is proposed to exploit the unique data structure and yield high resolution. The continuous motion of the object is utilized effectively.

Zusammenfassung. Ein inverses Synthetik-Apertur-Radarsystem, das zur Abbildung eines sich kontinuierlich bewegenden Objekts eingesetzt wird, soll untersucht werden. Es wird gezeigt, daß die Radarechos sich additiv aus zweidimensionalen komplexen Exponentiellen über einer kleinen Datenapertur zusammensetzen. Ein Matrix-Pencil-Verfahren wird vorgeschlagen, das die spezifische Datenstruktur ausnutzt und eine hohe Auflösung liefert. Die kontinuierliche Objektbewegung wird auf wirksame Weise genutzt.

Résumé. Nous étudions un radar à ouverture synthétique inverse à fréquence par paliers dans le contexte de la visualisation d'un objet se mouvant continuement. Nous montrons que les retours radar sont constitués par la somme d'exponentielles complexes à deux dimensions sur une petite ouverture de données. Nous proposons une méthode de matrix pencil pour exploiter cette structure de données unique et obtenir une résolution élevée. Nous utilisons efficacement le mouvement continu de l'objet.

Keywords. High resolution imaging; stepped frequency radar; matrix pencil.

1. Introduction

Radar imaging is a technology which has gone through three decades of research and development. Some modern research trends in this area can be found in [1–3, 9, 10]. One important issue which still dominates the interests of many researchers is resolution. High resolution is desired almost in all radar images. The conventional approach to obtain high resolution is to increase the effective aperture of the collected data. The synthetic aperture radar (SAR) [1] is the best example. While this is very effective in some applications, the data aperture can be severely limited by a number of physical, as well as computational, constraints in other applications such as the inverse synthetic aperture radar (ISAR).

In a stepped frequency ISAR [2] the object to be imaged rotates around its center with respect to a stationary radar. At one aspect angle of the object, the radar transmits a sequence of stepped frequency pulses towards the object and receives the returned signals. At the next aspect angle of the object, the radar does the same thing. This process is repeated for a number of times. As a result, the radar actually collects a two-dimensional (2-D) data set. The first dimension is the stepped frequency of the radar, and the second is the

Correspondence to: Dr. Y. Hua, Department of Electrical Engineering, University of Melbourne, Parkville, VIC 3052, Australia. E-mail yhua@mullian.ee.mu.oz.au

*This work was supported by the Australian Defence Science and Technology Organization (DSTO) and the Australian Research Council (ARC).

SSDI 0165-1684(93)E0040-R

rotation angle of the object. Both the frequency and the angular dimensions are limited by several factors as explained below. First, the reflection coefficients of many objects are frequency dependent as well as angle dependent. In order to describe such objects by images (at a nominal frequency band and a nominal looking angle), both the frequency and the angle ranges must be limited to be small. Second, the collected data with either large frequency range or large angle range can be too complicated to process to yield a good image within a given computing time. This often forces the data aperture which we can use to be small, so that the data satisfies a simple model and hence an efficient algorithm can be applied. For example, in [2], the frequency and angle ranges are chosen to be so small that the received data can be modelled by samples of the Fourier transform (of the object image) on rectangular coordinates, and hence the inverse fast Fourier transform (FFT) method can be applied. If the angle range is not very small, the radar returns are samples of the Fourier transform on polar coordinates, and hence (for computational efficiency) some interpolation methods must be used before the FFT can be applied.

In this paper, we will study a stepped frequency ISAR problem where the data aperture is so small that none of the FFT based methods can provide a satisfactory resolution. Specifically, we will consider an object which moves continuously (rather than in steps as in [2, 12]) with both angular and radial motions. We will show that the radar returns can be modelled by a sum of 2-D complex exponentials for a very small data aperture. To utilize the small aperture of data without loss of resolution, we will propose a matrix pencil method. This method retrieves the desired parameters (such as 2-D frequencies) from the radar returns more efficiently than other high resolution methods such as the maximum entropy and minimum variance [8]. This is because a searching in 2-D space is required by those methods but not the matrix pencil method.

In Section 2, the model for the radar returns will be discussed in detail. The 2-D complex exponentials will be shown to be the valid model over a small data aperture. It will be shown that the 2-D frequencies in the model are linearly related to the positions of the point scatterers in the object, and once the radial and rotational velocities of the object are known or estimated, they can be used to obtain the exact scatterer positions, i.e., the radar image. (At microwave frequencies, many objects can be viewed as clusters of point scatterers.) In Section 3, we will present the matrix pencil method for retrieving the 2-D frequencies from the radar returns. In Section 4, the high resolution capability of the matrix pencil method will be illustrated by a computer simulation in comparison to the FFT method.

2. The data model

The coordinate system of a moving object is shown in Fig. 1 with respect to a stationary radar. At any given time t, the motion of the object can be completely described by three components. The first component is the angular rotation of the object around a reference point in the object. The second is the radial motion of the reference point (or the object) along the line of sight of the radar. The third is the tangential motion of the reference point (or the object) which is perpendicular to the radial motion.

For a small angular change of the object and a narrow frequency bandwidth at microwave frequencies, the moving object is assumed to consist of a number of point scatterers each of which has a constant reflection coefficient. Then the complex envelope of a radar return can be described by

$$s(t) = \sum_{i=1}^{I} a_i \exp\left(-\mathrm{j}\frac{4\pi}{c} f(t) r_i(t)\right), \tag{2.1}$$

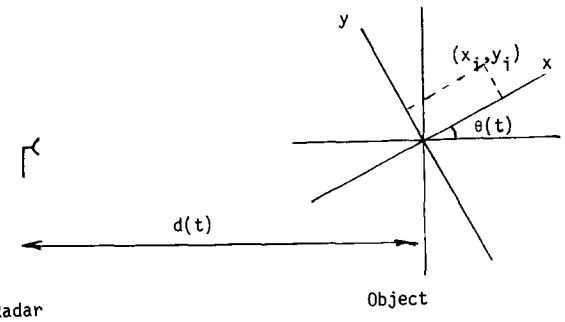

Fig. 1. The coordinate system of the moving object (in $x-y$) with respect to the radar.

where I is the number of scatterers, a_i the (complex) reflection coefficient (incorporating the phase and amplitude of the transmitted signal and the attenuation along the wave path), c the wave velocity, $f(t)$ the radar frequency, and $r_i(t)$ the distance between the radar and the i-th scatterer. The phase $(4\pi/c)f(t)r_i(t)$ is due to the round trip travel between the radar and the i-th scatterer. When the object is in the far field, we have

$$r_i(t) = d(t) + x_i \cos(\theta(t)) + y_i \sin(\theta(t)) , \tag{2.2}$$

where $d(t)$ is the distance between the radar and the reference point in the object, $\theta(t)$ the rotation angle, and (x_i, y_i) the position of the i-th scatterer. If the whole observation time is short, the moving object remains in the radar beam width, the distance $d(t)$ changes with a constant radial velocity v, i.e.,

$$d(t) = d_0 + vt , \tag{2.3}$$

and the angle $\theta(t)$ changes with a constant speed ω, i.e.,

$$\theta(t) = \omega t . \tag{2.4}$$

Note that the tangential motion of the object contributes nothing to the radar returns as long as the object is in the radar beam width. The initial angle is assumed to be zero without any loss of the geometry of the object. When the angular change is small, then $r_i(t)$ can be written as

$$\begin{aligned} r_i(t) &= d(t) + x_i - y_i\theta(t) \\ &= d_0 + vt + x_i - y_i\omega t . \end{aligned} \tag{2.5}$$

The radar transmits the stepped frequency pulses with the initial frequency f_0 and the frequency step Δf as shown in Fig. 2. Let Δt be the time interval between pulses, M the number of frequency steps from the lowest frequency f_0 to the highest frequency f_u and N the number of sweeps from f_0 to f_u. Then we can express the sampling time by $t = (nM + m)\Delta t$, where $m = 0,1, \ldots, M-1$ and $n = 0,1, \ldots, N-1$. Using this expression, we can write

$$f(t) = f_0 + \Delta f m , \tag{2.6}$$

$$r_i(t) = d_0 + v(nM + m)\ \Delta t + x_i - y_i\omega(nM + m)\ \Delta t .$$

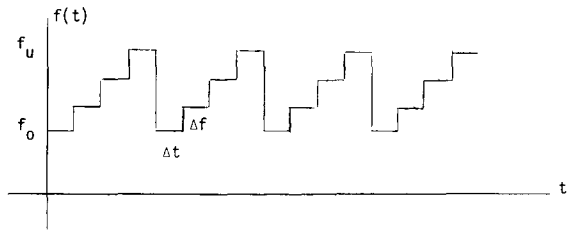

Fig. 2. The frequency of the stepped frequency ISAR as function of time.

(2.7)

(Note that strictly speaking, we have assumed that the object can be viewed to be stationary during the pulse interval which can be smaller but no larger than the sampling interval Δt.) Using (2.6) and (2.7) in (2.1), we now write

$$\begin{aligned} s(t) &= s(m,n) \\ &= \sum_{i=1}^{I} a_i \exp\left(-\mathrm{j}\frac{4\pi}{c}\phi_0(m) - \mathrm{j}\frac{4\pi}{c}\phi_i(m,n)\right), \end{aligned} \tag{2.8}$$

where

$$\phi_0(m) = d_0(f_0 + \Delta f m) , \tag{2.9}$$

$$\begin{aligned} \phi_i(m,n) = {} & f_0 x_i + f_0(v - y_i\omega)\Delta t\, m + f_0(v - y_i\omega)\Delta t\, Mn \\ & + \Delta f x_i m + \Delta f\,(v - y_i\omega)\,\Delta t\, m^2 \\ & + \Delta f(v - y_i\omega)\ \Delta t\, Mmn. \end{aligned} \tag{2.10}$$

Note that $\phi_0(m)$ can be compensated (i.e., removed) if the initial distance d_0 is known. If d_0 is unknown but an estimate d_0' is given, then the corresponding $\phi_0'(m)$ due to d_0' can be compensated and the difference $d_0 - d_0'$ is added to x_i. If $d_0 - d_0'$ is not so large to cause ambiguity, it only causes a translation of the whole object in the x-direction.

In (2.10), the second last term (of m^2) is negligible in the m-direction compared to the second term provided that the radar frequency bandwidth is very narrow, i.e., $B_T \ll f_0$ where $B_T = M\,\Delta f$. The last term (of mn) is negligible in the n-direction compared to the third term given $B_T \ll f_0$. However, the last term is not negligible in the m-direction compared to the second term unless

$$NB_T \ll f_0 . \tag{2.11}$$

Although $NB_T \ll f_0$ is more restrict than $B_T \ll f_0$, it still can be easily satisfied in practice. But it may imply that N must be small.

Neglecting $\phi_0(m)$ and the second last and last terms in $\phi_i(m,n)$, the radar returns can be rewritten as

$$s(m,n) = \sum_{i=1}^{I} b_i \exp(j\omega_{mi} m + j\omega_{ni} n) , \tag{2.12}$$

where

$$b_i = a_i \exp\left(-j \frac{4\pi}{c} f_0 x_i\right), \tag{2.13}$$

$$\omega_{mi} = -\frac{4\pi}{c} (f_0(v - y_i\omega)\ \Delta t + \Delta f\, x_i), \tag{2.14}$$

$$\omega_{ni} = -\frac{4\pi}{c} f_0 (v - y_i\omega)\ \Delta t\, M, \tag{2.15}$$

Now we see that the radar returns are a sum of 2-D complex exponentials provided $NB_T \ll f_0$ (narrow frequency band) and $\omega MN\,\Delta t \ll 1$ (small angular change). Furthermore, we know that the i-th 2-D frequency $(\omega_{mi}, \omega_{ni})$ provides a direct information about (x_i, y_i) the position of the i-th scatterer. Although ω_{mi} and ω_{ni} are not simple proportions of x_i (range) and y_i (cross-range), respectively, they are linearly related to each other. When v and ω are known or estimated, (x_i, y_i) can be retrieved from $(\omega_{mi},\omega_{ni})$ as follows:

$$x_i = \frac{c}{4\pi\ \Delta f}\left(\frac{\omega_{ni}}{M} - \omega_{mi}\right), \tag{2.16}$$

$$y_i = \frac{c}{4\pi f_0 \omega\ \Delta t\, M}\omega_{ni} + \frac{v}{\omega} . \tag{2.17}$$

Note that the error in radial velocity (if not so large to cause ambiguity) would introduce a constant shift in the cross range, and the error in angular velocity would introduce a scaling in the cross range. The range dimension is robust to these errors. Also note that there is no 'range walk' problem [1] here because we use a small data aperture.

In the next section, we will present the matrix pencil method for estimating the 2-D frequencies $(\omega_{mi},\omega_{ni})$ as well as the corresponding amplitudes b_i from $s(m,n)$.

3. Matrix pencil method

Given the model shown in (2.12), several methods [8] are available to find the 2-D frequencies and the corresponding amplitudes. But the matrix pencil method we will now present is computationally more efficient. This is because a searching procedure in 2-D space, which is not required by the matrix pencil method, must be carried out by other methods. We note that the concept of matrix pencil was previously used for 1-D superimposed exponentials [6] and recently used for a 2-D case [5]. A near optimum accuracy (compared to the Cramer–Rao bound) has been found for the matrix pencil approach in both 1-D [6] and 2-D [5] cases. But the version shown in [5] as well as in [12] requires more computations than the version shown below although they have a similar accuracy [11]. (An enhanced matrix to be proposed here is much smaller than that proposed in [5] which accounts for the computational efficiency of this version.)

We first rewrite (2.12) into the form

$$s(m,n) = \sum_{j=1}^{J} \sum_{k=1}^{K} b_{jk}\, p_j^m q_k^n , \tag{3.1}$$

where $\{p_j: j = 1, \ldots, J\}$ are all the distinct elements from $\{\exp(j\omega_{mi}: i = 1, \ldots, I\}$, $\{q_k: k = 1, \ldots, K\}$ all the distinct elements from $\exp(j\omega_{ni}): i = 1, \ldots, I\}$, $\{b_{jk}: j = 1, \ldots, J;\ k = 1, \ldots, K\}$ consist of $\{b_i: i = 1, \ldots, I\}$ and zeros. Clearly, the number of nonzero b_{jk} is I, the number of scatterers . Because of the zero b_{jk}, redundancy is introduced into the model. But it is the redundancy that leads to the matrix pencil method to be shown. In addition, we feel that the redundancy also tends to absorb some amount of model errors or noise and hence leave the real scatterer components less perturbed. We note that J and K can be estimated as will be mentioned again, and I can then be estimated by the number of dominant b_{jk}.

Now we put $s(m,n)$ into the matrix form:

$$\boldsymbol{S} = \boldsymbol{PBQ}^T , \tag{3.2}$$

where the superscript T denotes the transpose, and

$$\boldsymbol{P}=\begin{bmatrix} 1 & 1 & \cdots & 1 \\ p_1 & p_2 & \cdots & p_J \\ \vdots & \vdots & \cdots & \vdots \\ p_1^{M-1} & p_2^{M-1} & \cdots & p_J^{M-1} \end{bmatrix}, \tag{3.3}$$

$$\boldsymbol{B}=\begin{bmatrix} b_{11} & b_{12} & \cdots & b_{1K} \\ b_{21} & b_{22} & \cdots & b_{2K} \\ \vdots & \vdots & \cdots & \vdots \\ b_{J1} & b_{J2} & \cdots & b_{JK} \end{bmatrix}, \tag{3.4}$$

$$\boldsymbol{Q}=\begin{bmatrix} 1 & 1 & \cdots & 1 \\ q_1 & q_2 & \cdots & q_k \\ \vdots & \vdots & \cdots & \vdots \\ q_1^{N-1} & q_2^{N-1} & \cdots & q_K^{N-1} \end{bmatrix}. \tag{3.5}$$

When $\boldsymbol{P}$ and $\boldsymbol{Q}$ are available, the matrix $\boldsymbol{B}$ can simply be found by (the least-square solution)

$$\boldsymbol{B}=\boldsymbol{P}^{+}\boldsymbol{S}\boldsymbol{Q}^{+\mathrm{T}}, \tag{3.6}$$

where the superscript $^+$ denotes the pseudoinverse, i.e.,

$$\boldsymbol{P}^{+}=(\boldsymbol{P}^{\mathrm{H}}\boldsymbol{P})^{-1}\boldsymbol{P}^{\mathrm{H}}, \tag{3.7}$$

$$\boldsymbol{Q}^{+}=(\boldsymbol{Q}^{\mathrm{H}}\boldsymbol{Q})^{-1}\boldsymbol{Q}^{\mathrm{H}}. \tag{3.8}$$

The superscript H denotes the conjugate transpose. The inverse used in (3.7) and (3.8) implies that J and K are assumed to be no larger than M and N, respectively. Note that each nonzero element $|b_{jk}|$ in $\boldsymbol{B}$ represents the amplitude of the reflection coefficient of the point scatterer with the location defined by the corresponding p_j and q_k. The location defined by any pair of p_j and q_k can be computed by using

$$\omega_m=\mathrm{Im}[\log p_j], \tag{3.9}$$

$$\omega_n=\mathrm{Im}[\log q_k], \tag{3.10}$$

in place of ω_{mi} and ω_{ni} in (2.16) and (2.17). Im[ ] denotes the imaginary part. If p_j and q_k are estimated values, we found that forcing them to have the unit amplitudes stabilizes the computation of $\boldsymbol{B}$ using (3.6).

To show how to find p_j and q_k, we will focus on p_j only. This is because the role played by p_j is the same as that by q_k once m and j are exchanged by n and k, respectively. The whole procedure can be put into four steps as follows.

The first step is to form the enhanced matrix:

$$\boldsymbol{S}_{\mathrm{efb}}=[\boldsymbol{S}_e,\boldsymbol{P}\boldsymbol{S}_e^{*}], \tag{3.11}$$

where the superscript * denotes the complex conjugation, $\boldsymbol{P}$ is the permutation matrix with ones on its anti-diagonal axis, and

$$\boldsymbol{S}_{\mathrm{e}}=[\boldsymbol{S}_0,\boldsymbol{S}_1,\ \ldots,\boldsymbol{S}_{N-L}], \tag{3.12}$$

where $\boldsymbol{S}_i$ consists of the $(i+1)$th through $(i+L)$th rows of $\boldsymbol{S}$. L is a free integer to be discussed later. Using (3.2) and (3.3) together with (3.11), one can verify

$$\boldsymbol{S}_{\mathrm{efb}}=\boldsymbol{P}_L[\boldsymbol{Q}_{\mathrm{f}},\boldsymbol{P}_0^{*L-1}\boldsymbol{Q}_{\mathrm{f}}^{*}], \tag{3.13}$$

where

$$\boldsymbol{P}_L=\begin{bmatrix} 1 & 1 & \cdots & 1 \\ p_1 & p_2 & \cdots & p_J \\ \vdots & \vdots & \cdots & \vdots \\ p_1^{L-1} & p_2^{L-1} & \cdots & p_J^{L-1} \end{bmatrix}, \tag{3.14}$$

$$\boldsymbol{P}_0=\mathrm{diag}[p_1,p_2,\ \ldots,p_J], \tag{3.15}$$

$$\boldsymbol{Q}_{\mathrm{f}}=[\boldsymbol{B}\boldsymbol{Q}^{\mathrm{T}},\boldsymbol{P}_0\boldsymbol{B}\boldsymbol{Q}^{\mathrm{T}},\ \ldots,\boldsymbol{P}_0^{N-L}\boldsymbol{B}\boldsymbol{Q}^{\mathrm{T}}]. \tag{3.16}$$

It can be shown (see Appendix A) that if

$$J\leqslant L\leqslant N-J+1, \tag{3.17}$$

then

$$\mathrm{range}(\boldsymbol{S}_{\mathrm{efb}})=\mathrm{range}(\boldsymbol{P}_L). \tag{3.18}$$

The second step is to compute the matrix $\boldsymbol{U}$ of the J principal left singular vectors of $\boldsymbol{S}_{\mathrm{efb}}$. From (3.18) we know that

$$\mathrm{range}(\boldsymbol{U})=\mathrm{range}(\boldsymbol{P}_L), \tag{3.19}$$

or equivalently

$$\boldsymbol{U}=\boldsymbol{P}_L\boldsymbol{T}, \tag{3.20}$$

where $\boldsymbol{T}$ is a unique $J\times J$ nonsingular matrix.

The third step is to form the matrix pencil $\boldsymbol{U}_1-p\boldsymbol{U}_2$, where $\boldsymbol{U}_1$ is $\boldsymbol{U}$ without the first row, and $\boldsymbol{U}_2$ is $\boldsymbol{U}$ without the last row. Using (3.19), one can verify

$$\boldsymbol{U}_1-p\boldsymbol{U}_2=(\boldsymbol{P}_1-p\boldsymbol{P}_2)\boldsymbol{T}, \tag{3.21}$$

where $\boldsymbol{P}_1$ is $\boldsymbol{P}$ without the first row, and $\boldsymbol{P}_2$ is $\boldsymbol{P}$ without the last row. From (3.14), we know that

$$\boldsymbol{P}_1=\boldsymbol{P}_2\boldsymbol{P}_0, \tag{3.22}$$

and hence

$$\boldsymbol{U}_1 - p\boldsymbol{U}_2 = \boldsymbol{P}_2(\boldsymbol{P}_0 - p\boldsymbol{I})\boldsymbol{T}\,. \tag{3.23}$$

To ensure that the $(L-1)$-row matrix $\boldsymbol{P}_2$ also has the full rank J, we must modify (3.17) as

$$J+1 \leqslant L \leqslant N-J+1\,. \tag{3.24}$$

Then, a simple analysis [6] of (3.23) can show that $\{p_j; j=1, \ldots, J\}$ are the generalized eigenvalues (rank reducing numbers) of the matrix pencil $\boldsymbol{U}_1 - p\boldsymbol{U}_2$.

The final step is to compute the generalized eigenvalues of $\boldsymbol{U}_1 - p\boldsymbol{U}_2$ by computing the eigenvalues of $(\boldsymbol{U}_2^{\mathrm{H}}\boldsymbol{U}_2)^{-1}\boldsymbol{U}_2^{\mathrm{H}}\boldsymbol{U}_1$, For more discussions on the generalized eigenvalue problem, see [7].

Note that the effect of the free parameter L on the noise sensitivity is great but similar to that for the 1-D sinusoidal case shown in [6]. Good choices of L are between $N/3$ and $2N/3$. The choice of J follows from a property of $\boldsymbol{S}_{\mathrm{efb}}$, i.e., $\mathrm{rank}(\boldsymbol{S}_{\mathrm{efb}}) = J$. For noisy data, J should be the number of the dominant singular values of $\boldsymbol{S}_{\mathrm{efb}}$.

Also note that although the matrix pencil method was motivated by the small size of the available data set, it works as well on a large data set. In fact, for a large data set, the matrix pencil method can be more efficient in computation than the FFT method. To justify this, we can show (using some results in [4] that the total number of multiplications required by the matrix pencil method is in the order of $4L(N-L/2)N+10L^3$, assuming $M=N$ and $N>L \gg \max(J,K)$. The condition $L \gg \max(J,K)$ means that the image is sparse or composed of a small number of scatterers. It is also known that the total number of multiplications required for a typical 2-D FFT method to produce a 2-D FFT spectrum alone is in the order of $N^2\log_2 N$, assuming $M=N$. This is in addition to the computations required to search the peak frequencies and amplitudes in the 2-D spectrum. If N is also much larger than L (or if $\log_2 N$ is larger than $4L$), then the 2-D FFT spectrum alone would be more expensive to obtain than the estimated frequencies and amplitudes by the matrix pencil method.

4. Computer simulation

To illustrate the performance of the matrix pencil method for radar imaging, we assume the following.

For radar:

$c = 3\times 10^8$ m/s,

$f_0 = 10$ GHz,

$\Delta f = 0.5$ MHz,

$\Delta t = 18$ μs,

$M = N = 32$.

For object:

$\omega = 5$ degrees/s,

$v = 1$ m/s,

for i from 1 to 8

$x_i = 10\cos(\frac{1}{4}\pi(i-1))$ in meters,

$y_i = 10\sin(\frac{1}{4}\pi(i-1))$ in meters,

$a_i = \exp(\mathrm{j}w_i)$,

where w_i is randomly distributed between $[-\pi, \pi]$;

$d_0 \gg 20$ meters.

Based on the above parameters, a 32×32 synthesized X-band stepped frequency ISAR data set was generated using (2.1) with $\phi_0(m)$ suppressed. We also added complex white Gaussian noise with SNR = 30 dB where $\mathrm{SNR} = 10\log_{10}(1/2\sigma^2)$ and $2\sigma^2$ is the noise variance. Note that the total angle change is $\omega\Delta t\, MN = 0.092$ degree, and the radar frequency bandwidth is $B_{\mathrm{T}} = \Delta f M = 0.0512\, f_0/N$.

Figure 3 shows the 2-D FFT amplitude spectrum of the data set, where the top 10 dB dynamic range (ratio of the peak value over the threshold) is shown. Due to the small data aperture, none of the eight scatterers can

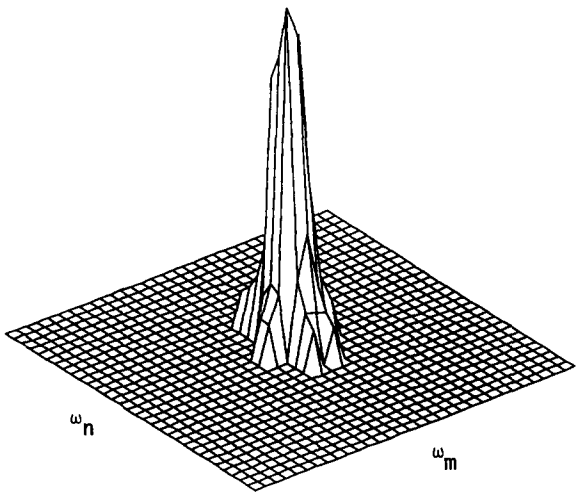

Fig. 3. The FFT amplitude spectrum of the synthesized X-band stepped frequency ISAR data.

be seen in this spectrum. From this spectrum, we can only tell a strong cluster of scatterers present.

Figure 4 shows the line spectrum defined by $|b_{jk}|$ versus the corresponding x_i and y_i which were obtained by the matrix pencil method with $L=15$ and J (or K) $=7$. From this spectrum (with the dynamic range 10 dB), we clearly see eight dominant scatterers and six other (weak) extraneous scatterers. The amplitudes and positions of the eight dominant scatterers are shown in Fig. 5. They are all close to the true values.

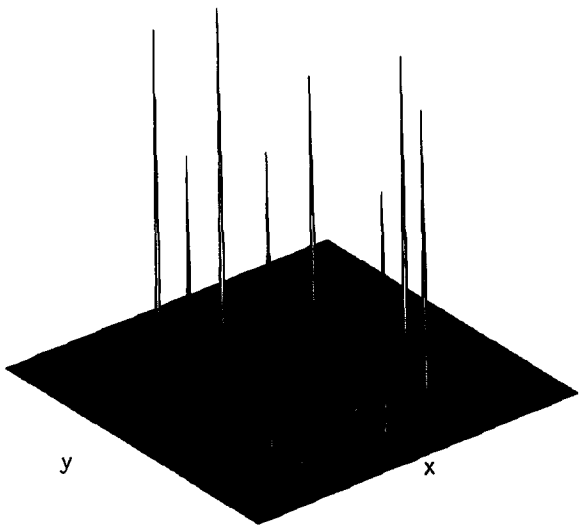

Fig. 4. The line spectrum obtained by the matrix pencil method of the same ISAR data.

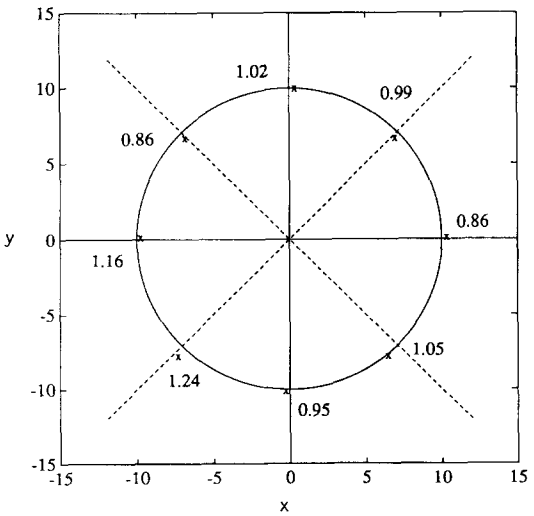

Fig. 5. The amplitudes and locations of the scatterers obtained by the matrix pencil method.

5. Conclusions

A high resolution method has been proposed for stepped frequency ISAR imaging of continuously moving object. This method called the matrix pencil method has been shown to provide much higher resolution than the conventional FFT method. The continuous motion of the moving object can be utilized effectively by applying the matrix pencil method to a small data aperture. More extensive simulation results of this method are documented in [11].

Appendix A

To prove (3.18), we let $\boldsymbol{S}_{e,k}$ be a submatrix of $\boldsymbol{S}_e$, consisting of the k-th column of each of $\boldsymbol{S}_0, \boldsymbol{S}_1, \ldots, \boldsymbol{S}_{N-L}$. Using (3.13) and (3.16), one can verify

$$\boldsymbol{S}_{e,k} = \boldsymbol{P}_L[\boldsymbol{c}_k, \boldsymbol{P}_0\boldsymbol{c}_k, \ldots, \boldsymbol{P}_0^{N-L}\boldsymbol{c}_k]$$
$$= \boldsymbol{P}_L\boldsymbol{C}_k\boldsymbol{P}_{N-L+1}^{\mathrm{T}}, \qquad \text{(A.1)}$$

where $\boldsymbol{c}_k = [c_{1k}, c_{2k}, \ldots, c_{Jk}]^{\mathrm{T}}$ is the k-th column of $\boldsymbol{BQ}^{\mathrm{T}}$,

$$\boldsymbol{C}_k = \mathrm{diag}[c_{1k}, c_{2k}, \ldots, c_{Jk}], \qquad \text{(A.2)}$$

and $\boldsymbol{P}_{N-L+1}$ is defined as $\boldsymbol{P}_L$ but with $N-L+1$ rows. Given $J \leqslant L$ and $J \leqslant N-L+1$ (i.e., given (3.17)), each of $\boldsymbol{P}_L$ and $\boldsymbol{P}_{N-L+1}$ has the full rank J (i.e., each of the J-column matrices $\boldsymbol{P}_L$ and $\boldsymbol{P}_{N-L+1}$ has J independent columns). Since $\boldsymbol{B}$ has no zero-row (otherwise, the number J would be reduced) and $\boldsymbol{Q}$ has K independent columns ($K \leqslant N$ is naturally assumed), each row of $\boldsymbol{BQ}^{\mathrm{T}}$ has at least one nonzero element. Let $c_{j,k(j)}$ be a nonzero element of $\boldsymbol{BQ}^{\mathrm{T}}$, which is on the j-th row and the $k(j)$-th column. Then, according to (A.1), range$(\boldsymbol{S}_{e,k(j)})$ belongs to range$(\boldsymbol{P}_L)$ and it must have a nonzero projection onto the j-th column of $\boldsymbol{P}_L$. It follows that

$$\mathrm{range}(\boldsymbol{S}_{e,k(1)}, \boldsymbol{S}_{e,k(2)}, \ldots, \boldsymbol{S}_{e,k(J)}) = \mathrm{range}(\boldsymbol{P}_L). \qquad \text{(A.3)}$$

Since the matrix $[S_{e,k(1)}, S_{e,k(2)}, \ldots, S_{e,k(J)}]$ consists of a subset of the columns of S_{efb}, therefore, (3.18) is proven.

Acknowledgments

The author would like to thank Mr. F. Baqai for making some figures shown in this paper.

References

[1] D.A. Ausherman, A. Kozma, J.L. Walker, H.M. Jones and E.C. Poggio, "Developments in radar imaging", *IEEE Trans. Aerospace Electron. Systems*, Vol. 20, No. 4, July 1984, pp. 363–400.

[2] C.C. Chen and H.C, Andrews, "Multifrequency imaging of radar turntable data", *IEEE Trans. Aerospace Electron. Systems*, Vol. 16, January1980, pp. 15–22.

[3] N.H. Farnat and B. Bai, "Optimal spectral windows for microwave diversity imaging", *IEEE Trans. Antennas and Propagation*, Vol. 39, No. 7, July 1991, pp. 985–993.

[4] G.H. Golub and C.F. Van Loan, *Matrix Computations*, Johns Hopkins Univ. Press, Baltimore, MD, 1983.

[5] Y. Hua, "Estimating two-dimensional frequencies by matrix enhancement and matrix pencil", *Proc. Internat. Conf. Acoust. Speech Signal Process. 91*, Ontario, Canada, May 1991; Full version in: *IEEE Trans. Signal Process.*, Vol. 40, No. 9, September 1992, pp. 2267–2280.

[6] Y. Hua and T.K. Sarkar, "Matrix pencil method for estimating parameters of exponentially damped/undamped sinusoids in noise", *IEEE Trans. Acoust. Speech Signal Process.*, Vol. 38, No. 5, May 1990, pp. 814–824.

[7] Y. Hua and T.K. Sarkar, "On SVD for estimating generalized eigenvalues of singular matrix pencil in noise", *IEEE Trans. Signal Process.*, Vol. 39, No. 4, April 1991, pp. 892–900.

[8] L. Marple, *Digital Spectral Analysis with Applications*, Prentice Hall, Englewood Cliffs, NJ, 1988.

[9] D.C. Munson and R.L. Visentin, "A signal processing view of strip-mapping synthetic aperture radar", *IEEE Trans. Acoust. Speech Signal Process.*, Vol. 37, No. 12, December 1989, pp. 2131–2147.

[10] B.D. Steinberg, "Microwave imaging of aircraft", *Proc. IEEE*, Vol. 76, No. 12, December 1988, pp. 1578–1592.

[11] F. Bagai, Matrix pencil methods for 2-D frequency estimation and ISAR imaging, Master Thesis, University of Melbourne, Australia, 1992.

[12] Y. Hua, F. Bagai, Y. Zhu and D. Heilbronn, "Imaging of point scatterers from step-frequency ISAR data", *IEEE Trans. Aerospace Electron. Systems*, Vol. 29, No. 1, January 1993, pp. 195–205